

Supplementary Information for:

Automated design of efficient and functionally diverse enzyme repertoires

Khersonsky et al.

Supplemental Tables

Tables S1 and S5 are supplied as individual Excel sheets.

Table S2. Activity of PTE variants with nerve agents of V type, k_{cat}/K_M s⁻¹M⁻¹.

Related to Figure 2.

Variant	VX		RVX	
	S-isomer	R-isomer	S-isomer	R-isomer
PTE S5	157±12	113±3	10.0±1.6	333±22
dPTE2	317±67	400±12	217±67	1833±167
PTE_3	141.7	40	1650	<16
PTE_4	250.0	110	1567	<16
PTE_7	<16	30	18	<16
PTE_9	35	183	23	<16
PTE_10	60	72	18	<16
PTE_13	152±1	62	50	500
PTE_24	116±10	650±47	100	NM
PTE_26	<16	18	<16	<16
PTE_27	11,000±2333	4000±167	333±166	11,500±1000
PTE_28	700±50	<25	15,500±1167	<25

PTE_29	666±166	333±166	5500±500	210
PTE_30	33		27	122
PTE_32	<16	133	<16	<16
PTE_33	<16		<16	<16
PTE_34	<16		<16	<16
PTE_27.4	35		283	<33
PTE_27.5	750		1133	<33
PTE_27.7	917		7500	833
PTE_27.10	4833		467	<33
PTE_27.13	483		8167	<33
PTE_27.14	717±100	<25	14670±1500	<25
PTE_27.16	250±50	<25	2667±117	<33
PTE_27.18	138		3000	<33
PTE_27.19	20		300	<33
PTE_27.22	45		67	<33
PTE_27.24	80		2667	<33
PTE_27.25	90		8167	<33
PTE_27.27	40		900	<33

Table S3. Comparison of best PTE designs activity with nerve agents with that of PTE variants obtained by directed evolution. $k_{cat}/K_M \times 10^6 \text{ M}^{-1}\text{min}^{-1}$, measured in 50 mM Tris with 50 mM NaCl at pH 8, 25°C. Related to Figure 2.

Variant	GF	GD	S-VX	S-RVX
PTE-S5 ^a	0.048±0.008 ^a	0.98±0.31 (0.11±0.03) ^{a,b}	0.0094 ^a	0.0006 ^a
	0.124±0.009 ^c	0.099±0.005 ^c	0.01 ^c	0.0009 ^c
dPTE2	0.170±0.003	0.29±0.06 (0.10±0.01)	0.019±0.004	0.013±0.004
PTE_27	1.06±0.11	0.11±0.017	0.66 ±0.14	0.02±0.01
PTE_28	191±36	3.9±0.2	0.042±0.003	0.93±0.07
PTE_27.14	159±19	31.2 ±14.0 (6.2±1.2)	0.043 ±0.006	0.88±0.09
PTE_27.16	136±18	119.5±4.9 (20.5±13.4)	0.015±0.003	0.16±0.7
C23 ^c	1.74±0.23	2.64±0.16	5.95±0.16	0.45±0.01
IV-A1 ^c	1.86±0.18	1.53±0.05	2.53±0.11	5.27±0.16
d1-IVA1 ^d PROSS stabilized		3.8 (1.1) ^b	3.5	12
10-2-C3 ^d stabilized		1.4 (0.2) ^b	50	3.2

^a Data for wt-PTE-S5 taken from Cherny et al (Cherny et al., 2013). Determined at 25°C, by use of both the DTNB and the loss of anti-AChE protocols.

^b In some cases, detoxification of the two S-enantiomers of GD was biphasic, which is attributed to the two toxic isomers, S_pC_R and S_pC_S. The parameters for the slow phase are given in the parentheses.

^c Data from Goldsmith et al (Goldsmith et al., 2016). All entries determined with authentic nerve agents at 37°C using the protocol of monitoring the anti-AChE loss of the OPs.

^d Data from Goldsmith et al (Goldsmith et al., 2017).

Table S4. Data collection and refinement statistics for the PTE designs. Related to Figure 4.

	PTE_5	PTE_27	PTE_28
Data Collection			
PDB code	6GBJ	6GBK	6GBL
Space group	$P4_32_12$	$C2$	$C2$
Cell dimensions:			
a,b,c (Å)	69.49 69.49 186.02	156.75 53.09 89.23	55.80 53.56 89.34
α,β,γ (°)	90, 90, 90	90, 106.81,90	90, 107.21, 90
No. of copies in a.u.	1	1	1
Resolution (Å)	38.65 -1.63	41.47-1.9	41.61-1.95
Upper resolution shell (Å)	1.69 -1.63	1.97 -1.9	2.02-1.95
Unique reflections	57,720 (5,611)	55,705 (5,523)	45,387 (3,967)
Completeness (%) Multiplicity	99.70 (98.79) 7.4(7.3)	99.91(99.87) 3.3(3.2)	87.83 (77.54) 7.4(7.3)
Average $I/\sigma(I)$	13.5(2.8)	5.56 (1.49)	10.91(3.05)
Rsym (I) (%)	0.0338(0.262)	0.09026 (0.4785)	0.0456(0.224)
Refinement			
Resolution range (Å)	38.65 -1.63	41.47-1.9	41.61-1.95
No. of reflections ($I/\sigma(I) > 0$)	57,716	55,668	45,382
No. of reflections in test set	2,886	2,783	2,272

R-working (%) / R-free (%)	0.1696/0.1891	0.2010/0.2182	0.1833/0.2253
No. of protein atoms	2,558	5,064	5063
No. of water molecules	330	659	660
Overall average B factor (\AA^2)	18.54	11.32	18.61
Root mean square deviations:			
- bond length (\AA)	0.025	0.011	0.018
- bond angle ($^\circ$)	2.36	1.53	1.85
Ramachandran Plot			
Most favored (%)	96.95	96.47	96.31
Additionally allowed (%)	3.05	3.53	3.69
Disallowed (%)	0.0	0.0	0.0

* Values in parentheses refer to the data of the corresponding upper resolution shell

Table S6. Specificity changes (as ratios of specific activity) in ACS variants.

Related to Figure 5.

ACS variant	Acetate/ Butyrate	Specificity switch relative to ACS_PROSS	Acetate/ Isobutyrate	Specificity switch relative to ACS_PROSS	Acetate/ Caproate	Specificity switch relative to ACS_PROSS
ACS_PROSS	22.5	1.0	44.4	1.0	29.8	1.0
ACS_3	27.2	0.8	50.6	0.9	75.9	0.4
ACS_4	13.8	1.6	2.4	18.8	25.3	1.2
ACS_9	5.5	4.1	0.9	46.9	33.5	0.9
ACS_10	11.1	2.0	3.0	14.8	13.8	2.2
ACS_14	0.3	87.9	0.6	76.9	0.7	45.9
ACS_16	2.3	9.7	2.0	22.5	8.4	3.6
ACS_19	12.3	1.8	10.7	4.1	11.8	2.5
ACS_27	3.2	7.1	0.7	64.8	4.9	6.1

Supplementary Figures

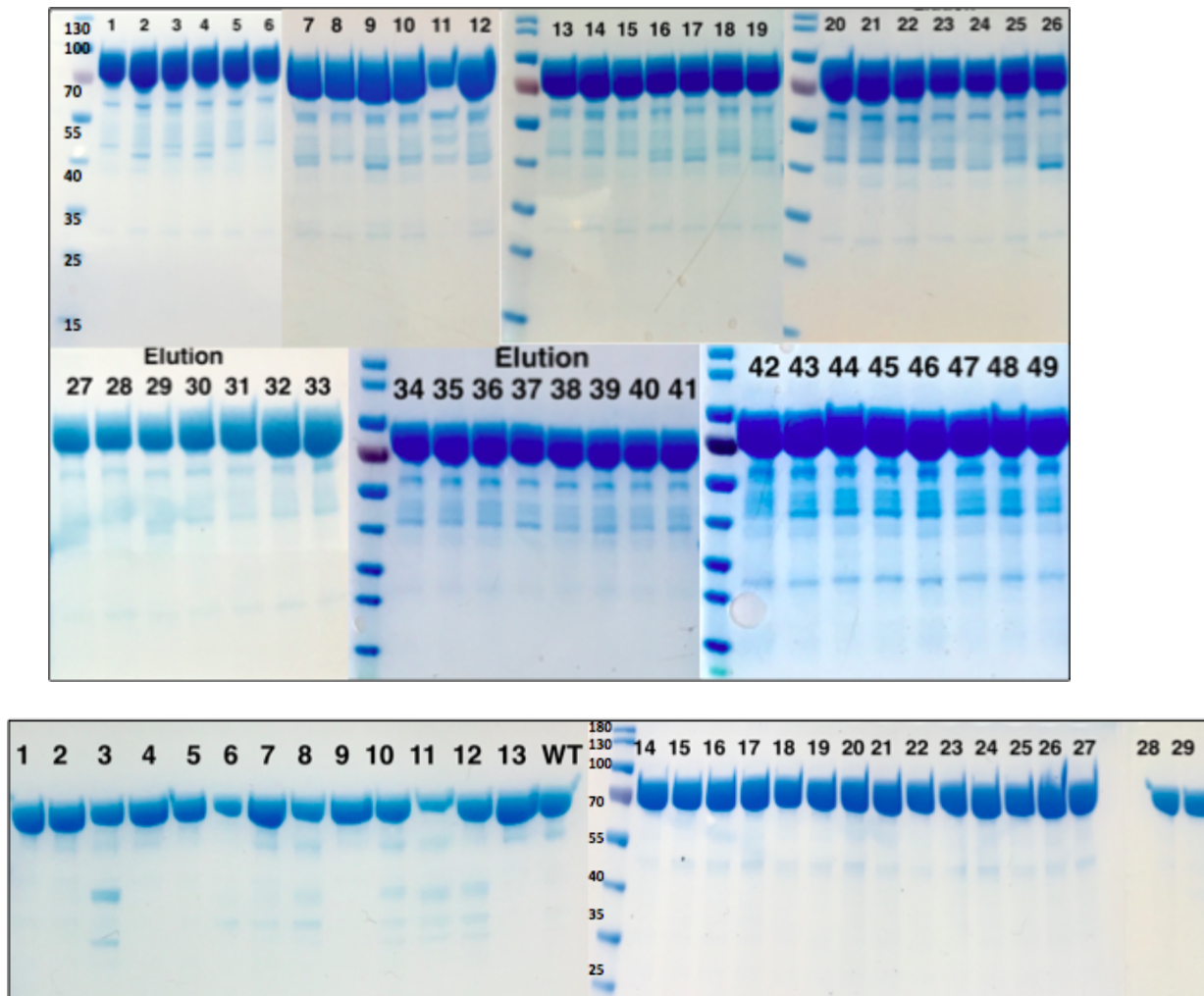


Figure S1. SDS-PAGE analysis FuncLib designs. Related to Figures 2 and 5. Top: PTE designs 1-49 after purification with amylose resin. Bottom: ACS designs 1-29 after purification with Ni-NTA resin.

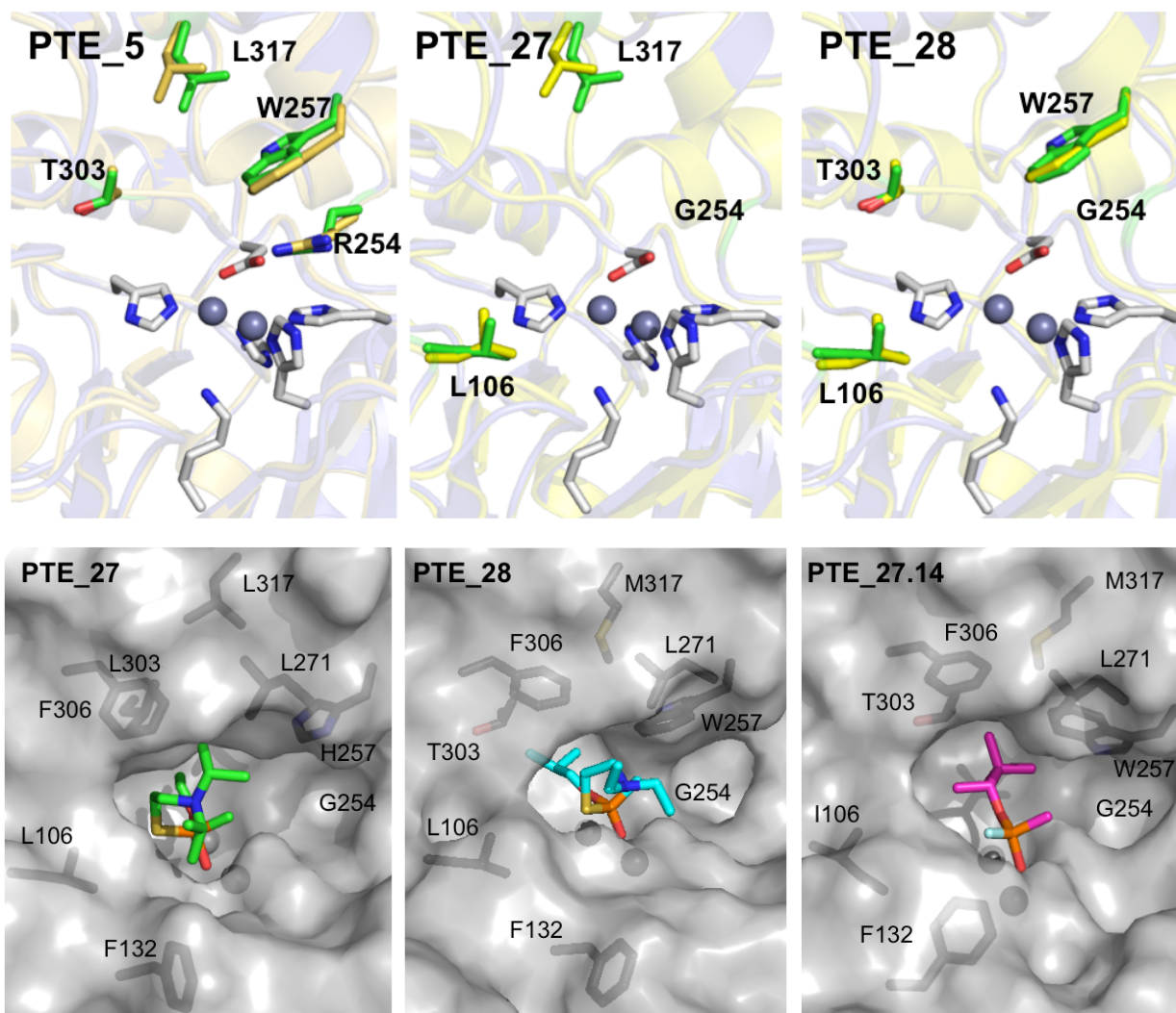


Figure S2. Top: Overlay of designed PTE crystal structures (yellow) and models (green).

Metal-chelating residues are shown as gray sticks, and Zn²⁺ ions as gray spheres.

Bottom: Catalytic poses of nerve agents in designed active-site pockets. Related to Figure 4.

The poses were obtained from docking simulations using the Adaptive-PELE method. Shown are S_p stereoisomers of VX, RVX, and GD in the active-site pockets of PTE_27, PTE_28, and PTE_27.14, respectively. The three models show high geometric complementarity between the designed pockets and the respective substrates. Designed residues and the substrates are shown as sticks and Zn²⁺ ions as gray spheres. The PTE_27 and PTE_28 poses were started from their respective X-ray crystallographic structures, and PTE_27.14 was started from the design model.

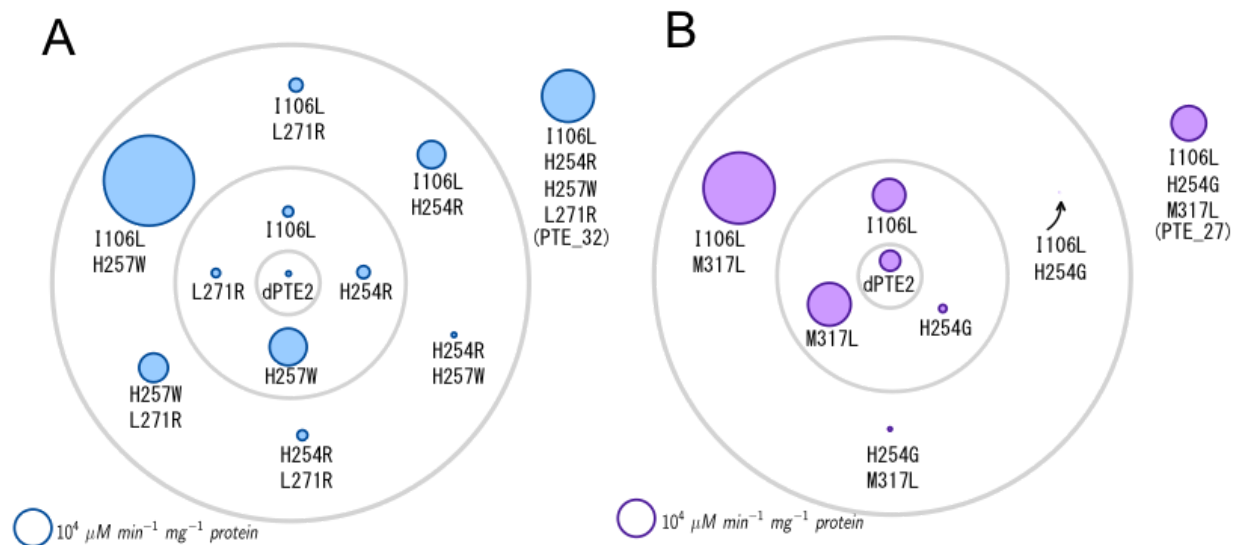


Figure S3. Epistasis among FuncLib mutations. Related to Figure 3. (A) PTE_32 (>100-fold improvement in esterase activity). (B) PTE_27 (65-fold improvement in lactonase activity). Circle sizes correspond to specific activities with 2-NA (A) and TBBL (B).

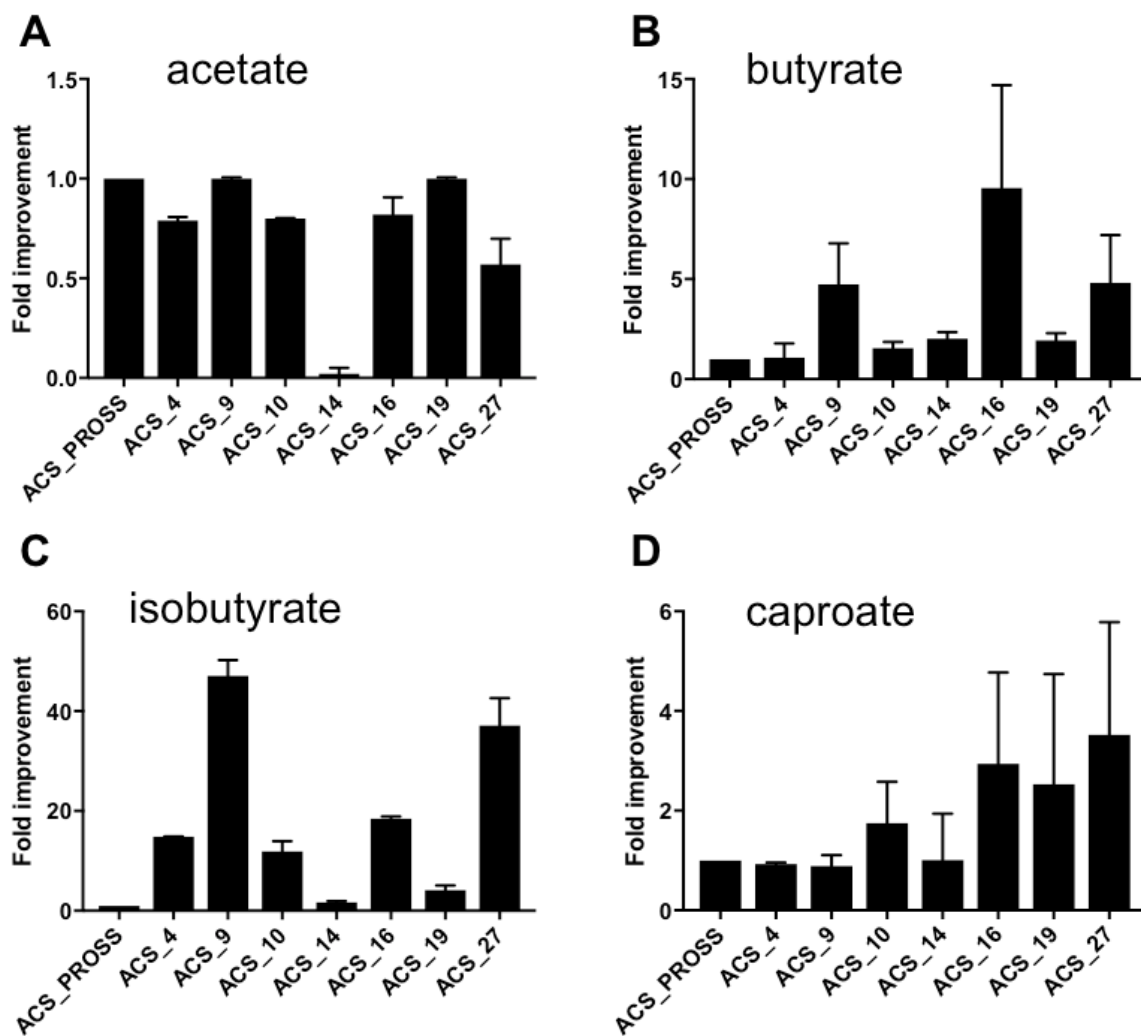


Figure S4. Fold improvement in specific activity of the best FuncLib ACS designs relative to ACS_PROSS with acetate (A), butyrate (B), isobutyrate (C), and caproate (D). Related to Figure 5.

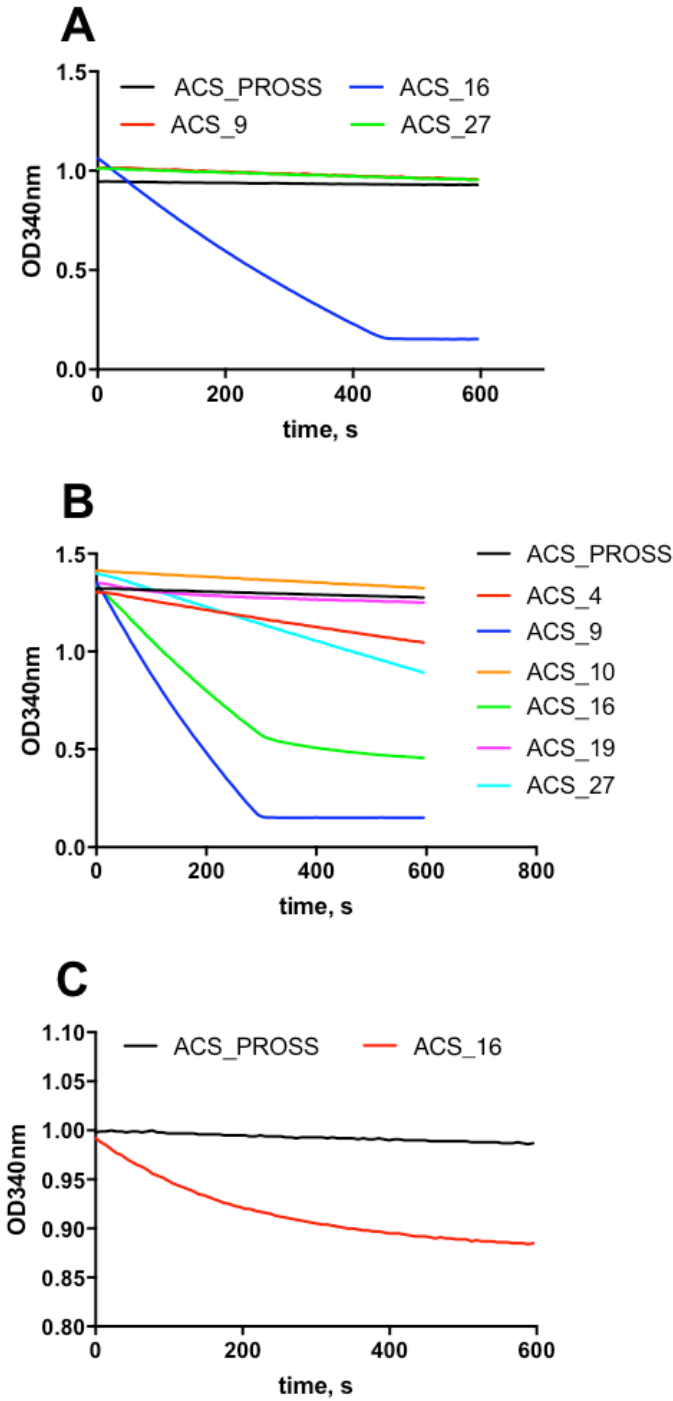


Figure S5. Kinetic traces of the ACS variants with 1mM butyrate (A), isobutyrate (B), and caproate (C), measured by the coupled assay (Reger et al., 2007). Related to Figure 5. ACS activity is coupled to NADH consumption, and larger decrease of OD at 340nm in FuncLib ACS designs relative to ACS_PROSS corresponds to higher activity.